Laminar Validation Cases for the Incompressible Flow Model in ALE3D

J. Ortega

July 16, 2002

DISCLAIMER

This report has been reproduced directly from the best available copy.

Available electronically at http://www.doc.gov/bridge

Available for a processing fee to U.S. Department of Energy
And its contractors in paper from
U.S. Department of Energy
Office of Scientific and Technical Information
P.O. Box 62
Oak Ridge, TN 37831-0062
Telephone: (865) 576-8401
Facsimile: (865) 576-5728
E-mail: reports@adonis.osti.gov

Available for the sale to the public from
U.S. Department of Commerce
National Technical Information Service
5285 Port Royal Road
Springfield, VA 22161
Telephone: (800) 553-6847
Facsimile: (703) 605-6900
E-mail: orders@ntis.fedworld.gov
Online ordering: http://www.ntis.gov/ordering.htm

OR

Lawrence Livermore National Laboratory
Technical Information Department's Digital Library
http://www.llnl.gov/tid/Library.html

Laminar Validation Cases for the Incompressible Flow Model in ALE3D

By

Jason Ortega
ortega17@llnl.gov

1.0 Overview

To benchmark the incompressible flow model in ALE3D[1], two test cases are conducted. The first case of two-dimensional flow over a flat plate is selected because it provides a straightforward example to determine whether or not ALE3D can grow a boundary layer by viscous diffusion. The benefit of the flat plate problem is that under certain conditions, the governing Navier-Stokes equations can be simplified and solved with numerical techniques, providing an independent result that can be compared with the solution from ALE3D. The second test case is that of two-dimensional, laminar flow about a circular cylinder. This test case is selected because it provides the complexity of an unsteady bluff-body wake in which vorticity is periodically shed from the surface of the cylinder. Since this canonical flow problem has been studied extensively both experimentally and computationally, the results from ALE3D can be compared with those presented in the literature.

The results for the flat plate case demonstrate that the implicit time integration scheme results in an approximate twenty-four-fold reduction of the simulation time over that of the explicit time integration scheme. On the other hand, a problematic trend is observed in the explicit time integration scheme used in the flat plate case. The errors in both the velocity and shear stress are not reduced through grid refinement as one might expect. Another trend that raises concern with the flat plate problem is the sensitivity of the velocity and shear stress to the outlet zero natural boundary condition. In all of the flat plate simulations, at least one of the calculated quantities varies quite noticeably near the outlet of the flow domain. For the case of a circular cylinder in which an explicit time integration scheme is employed, both the drag coefficient and Strouhal number demonstrate trends of converging to a solution that compares favorably with results from other studies in the literature.

2.0 Flow Over a Flat Plate

Prandtl[2] was the first to demonstrate the simplifications that can be made to the Navier-Stokes equations for external flow over a body at high Reynolds number, *Re*. What follows is a brief summary of Prandtl's simplifications. Due to the no-slip boundary condition at the body, there exists a thin layer of fluid, called the boundary

layer, in which the flow rapidly transitions from zero velocity at the wall to the free stream velocity, U_o, at the outer edge of the boundary layer. Consequently, steep velocity gradients ($\partial u / \partial y \gg 1$) exist in this layer and, hence, even small amounts of viscosity can result in a relatively large wall shear stress, $\tau_w = \mu \partial u / \partial y |_{y=0}$, where μ is the fluid viscosity and y is the coordinate value in the normal direction away from the wall. Outside the boundary layer, the flow is irrotational and inertial forces dominate the flow field. With this physical reasoning, the steady-state, two-dimensional Navier-Stokes equations

$$u\frac{\partial u}{\partial x} + v\frac{\partial u}{\partial y} = -\frac{1}{\rho}\frac{\partial p}{\partial x} + \nu\left(\frac{\partial^2 u}{\partial x^2} + \frac{\partial^2 u}{\partial y^2}\right) \tag{1}$$

$$u\frac{\partial v}{\partial x} + v\frac{\partial v}{\partial y} = -\frac{1}{\rho}\frac{\partial p}{\partial y} + \nu\left(\frac{\partial^2 v}{\partial x^2} + \frac{\partial^2 v}{\partial y^2}\right) \tag{2}$$

$$\frac{\partial u}{\partial x} + \frac{\partial v}{\partial y} = 0 \tag{3}$$

can be simplified by a scaling argument. It is assumed that $u \sim U_o, x \sim l, y \sim \delta, p \sim \rho U_o^2$, where U_o is the free stream velocity, l is the characteristic length of the body, δ is the boundary layer thickness ($\delta / l \ll 1$), and ρ is the fluid density. Non-dimensionalizing the Navier-Stokes equations by these scaling factors and letting $Re_x = U_o x / \nu \gg 1$ reduces Eqs. 1-3 to

$$u\frac{\partial u}{\partial x} + v\frac{\partial u}{\partial y} = -\frac{1}{\rho}\frac{\partial p}{\partial x} + \nu\frac{\partial^2 u}{\partial y^2} \tag{4}$$

$$\frac{\partial p}{\partial y} = 0 \tag{5}$$

$$\frac{\partial u}{\partial x} + \frac{\partial v}{\partial y} = 0 \tag{6}$$

for steady state flow. At the outer edge of the boundary layer, Eq. 4 becomes

$$U_o\frac{\partial U_o}{\partial x} = -\frac{1}{\rho}\frac{\partial p}{\partial x} \tag{7}$$

Thus, the pressure gradient can be obtained from the irrotational free stream velocity, U_o. From Eq. 5, this same pressure gradient exists through the entire boundary layer. Eq. 4 can be further simplified for flow over a flat plate. In this case, the free stream velocity is given by $U_o = const.$, such that $\partial p / \partial x = 0$. Thus, as was shown by Blasius[3], Eq. 4 reduces to

2

$$u\frac{\partial u}{\partial x} + v\frac{\partial u}{\partial y} = v\frac{\partial^2 u}{\partial y^2} \qquad (8)$$

Introducing the similarity variable, $\eta = \dfrac{y}{\sqrt{vx/U_o}}$ and the streamfunction,

$\psi = \sqrt{U_o vx}\, f(\eta)$, Eqs. 6 and 7 reduce to a single third order, non-linear, ordinary differential equation,

$$ff''+2f'''=0 \qquad (9)$$

where $f(\eta=0) = 0$, $f'(\eta=0)=0$, and $f'(\eta\rightarrow\infty) = 1$. Solving Eq. 9 numerically yields the horizontal and vertical velocity profiles shown in Figure 2.1. The skin friction coefficient, C_f, is given by

$$C_f = \frac{\mu \partial u/\partial y|_{y=0}}{\frac{1}{2}\rho U_o^{\,2}} = 0.664/\sqrt{Re_x} \qquad (10)$$

It should be noted that neither the velocity profiles in Figure 2.1 nor C_f is applicable near the leading edge of the plate since the assumption of $Re_x \gg 1$ is not valid for small x.

(a)   (b)
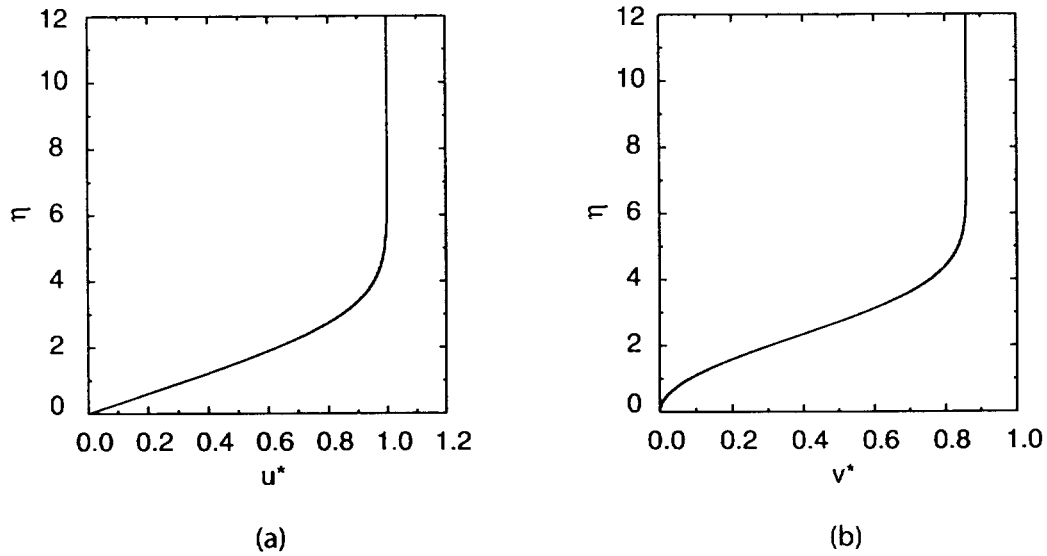
Figure 2.1. Horizontal and vertical velocity profiles from the numerical solution of Eq. 9. In these plots, $u^* = f'(\eta)$ and $v^* = v(\eta)/\sqrt{vU_o/x} = \frac{1}{2}(\eta f'-f)$.

2.1 Computational Setup

Simulations of two-dimensional flow over a flat plate are performed with the incompressible flow model in ALE3D, which numerically solves the Navier-Stokes equations using a Galerkin finite element method.[4,5] The ALE3D input files for these

3

simulations are shown in Appendix 1. To determine the sensitivity of the results to the grid resolution, two grids, coarse and medium, are chosen for this exercise (Figure 2.2). Table 1 describes the details of these two grids. Both an explicit and an implicit time-integration scheme are used in these simulations. The implicit scheme is used in this test case to determine its ability to decrease the simulation run time. Since the implicit scheme is not restricted by a numerically stable time step, it is capable of taking larger time steps than the explicit scheme. For the explicit simulations, the solution is advanced forward in time with a forward Euler time integration method. A projection method similar to that developed by Gresho *et al.* is used for the implicit solutions.[4]

A total of four simulations are performed for the flat plate test case: two simulations with the explicit scheme and two simulations with the implicit scheme. For the explicit scheme, the two simulations involve using the coarse and medium grids with the horizontal and vertical velocities specified at the inlet. The inlet velocity boundary conditions are chosen to be the horizontal and vertical velocity profiles of a Blasius boundary layer for $x_o = 1.0$, $U_o = 1.0$, and $\nu = 0.0005$, effectively giving an inlet Reynolds number of 2,000. Since $Re \gg 1$, the results of these simulations can be compared to the solution of the Blasius boundary layer problem. For the first simulation with the implicit scheme, only the horizontal velocity is specified at the inlet, while for the second simulation, both the horizontal and vertical velocities are specified at the inlet. This variation in the inlet boundary condition is done to determine the sensitivity of the solution to the inlet vertical velocity. When the vertical velocity component is left unspecified at the inlet, a zero natural boundary condition[1] on the tangential traction is used at the inlet. Only the medium grid is used for the implicit simulations. Again, the inlet velocity profiles are taken to be those of a Blasius boundary layer for for $x_o = 1.0$, $U_o = 1.0$, and $\nu = 0.0005$ for the implicit simulations. The following boundary conditions are common to both the explicit and implicit time-integration simulations. At the bottom wall ($y = 0$), the velocity boundary condition is one of no-slip and no-penetration. A zero natural boundary condition is imposed at the top and outlet of the computational domain. The out-of-plane velocity component, w, is set to zero for all of the nodes. No boundary conditions are needed for the pressure. The initial conditions at $t = 0$ are $u(x-x_o>, y>0) = 1.0$ and $v(x-x_o>0, y>0) = 0$. Internal to the code, this initial condition then is projected to a divergence-free field.[4] Table 2 summarizes the details of each of the four simulations. The CFL number is taken to be 0.5 for both grids in the explicit simulations.

In the implicit scheme, the CFL number for the advection term is set to 3.0, while the stability number for the diffusion term is set to 10^6. Consequently, the time step in the implicit scheme simulations is not diffusion limited. For the explicit simulations, the governing equations are solved with a conjugate gradient solver with a tolerance set to 10^{-12}. For the implicit simulations, a conjugate gradient solver is used to solve the pressure Poisson equation and a generalized minimum residual solver (gmres) is used to solve the momentum equations. For both of these solvers, the tolerance is set to 10^{-12}. Since the vertical velocity field converges more slowly than the horizontal velocity field,
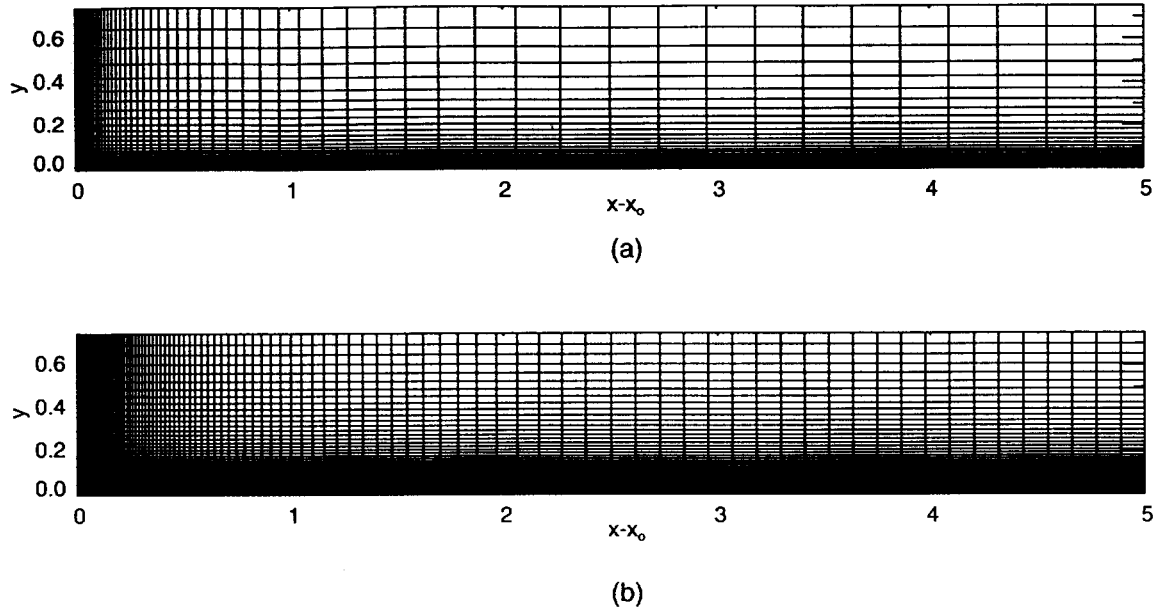
(a)

(b)

Figure 2.2. (a) Coarse and (b) medium grids used to simulate flow over a flat plate. The variable $x_o = 1.0$ is the offset of the computational domain from origin of the x axis.

Grid	Total Number of Elements	Number of Elements in x	Number of Elements in y	Δx_{min}	Δy_{min}
Coarse	2440	61	40	0.002152468	0.000419352
Medium	9760	122	80	0.001050609	0.000202344

Table 1. Details of the two grids used for the simulations of flow over a flat plate. The resolution is doubled in the x and y directions from the coarse to medium grid, such that the medium grid has four times as many elements as the coarse grid.

Run	Time-integration scheme	u_{inlet}	v_{inlet}
1	Explicit	Specified	Specified
2	Explicit	Specified	Specified
3	Implicit	Specified	Unspecified
4	Implicit	Specified	Specified

Table 2. Details of the four flat plate simulations.

5

the simulations are run until the absolute value of the relative change in the vertical velocity is less than 0.01%. Each of the simulations in Runs 1-3 are done on eight 375 MHz processors on an IBM SP machine. On the other hand, Run 4 is done on only one processor, making a direct timing comparison with Run 2 somewhat difficult. However, if the timing performance of Run 2 is simply multiplied by 8, it can be shown that the implicit time integration scheme runs approximately twenty-four times faster than the explicit time integration scheme for the case in which both the horizontal and vertical velocity components specified at the inlet. Post-processing and plotting of these simulations are done with Interactive Data Language (IDL) of Research Systems, Inc.

2.2 Results and Discussion

Plots of the horizontal velocity profiles and their relative differences with the Blasius horizontal velocity are shown in Figure 2.3. For both explicit cases (Runs 1-2), the maximum relative error in the horizontal velocity is approximately 1%. As the grid is refined from Run 1 to Run 2, the reduction in the maximum error of the horizontal velocity is small. This trend indicates that the solution is fairly insensitive to the grid resolution and that further grid refinement may not reduce the error in the horizontal velocity significantly below 1%. The error is somewhat smaller for the implicit simulations (Runs 3-4). For Run 3, the relative error is about 0.25%, while it is approximately 0.5% for Run 4. The profiles for the implicit cases exhibit noticeable dependence upon the chosen downstream location at which the profiles are taken, perhaps indicating sensitivity to the zero natural outlet boundary condition. Note that for Runs 1-2, and 4, in which both velocity components are specified at the inlet, ALE3D under predicts the horizontal velocity. However, for Run 3, in which only the horizontal velocity is specified at the inlet, ALE3D over predicts the values of the horizontal velocity. It can also be seen that specifying the vertical velocity in Run 4 results in a slightly greater error in the horizontal velocity than that in Run 3, where the inlet vertical velocity is unspecified.

The vertical velocity profiles (Figure 2.4) exhibit errors that are somewhat larger than those for the horizontal profiles. This observation is expected because the vertical velocity scales as $Re_x^{-1/2}$, making it significantly smaller than the horizontal velocity and more sensitive to errors in the numerical solution. For all four runs, the magnitude of the maximum error in the vertical velocity is approximately 3-4%. In addition, the errors for both the explicit and implicit time integration schemes are dependent upon the downstream location at which the comparison with the Blasius profile is made. The magnitude of the error in the vertical velocity is consistently greatest at the farthest downstream location, perhaps indicating sensitivity to the outlet zero natural boundary condition. For the explicit simulations, the trend is for the Navier-Stokes computations to overshoot the correct values in the vertical velocity. On the other hand, the Navier-Stokes computations undershoot the correct vertical velocity for both implicit simulations. As is the case for the horizontal profiles, grid refinement in Runs 1 and 2 does not result in a reduction of the vertical velocity error. Again, this trend is problematic since it suggests that further grid refinement may not result in further error reduction.

6

The shear stress coefficients and their relative errors are plotted in Figure 2.5. The computed values of C_f follow the general trend of Eq. 10. Though, it can be seen that the relative error in the shear stress coefficient has a maximum absolute value of approximately 2-4% over all four simulations. For the explicit cases, the relative error decreases from zero at the inlet and then exhibits oscillations near the outlet. Once again, the error in the shear stress coefficient does not decrease as the grid is refined in Runs 1 and 2. For the implicit cases, the relative error in C_f increases away from the inlet, decreases to a minimum, and then increases near the outlet. Unlike C_{ferr} for the explicit runs, C_{ferr} for the implicit runs are relatively smooth and do not exhibit oscillations. Note, however, that there is a sudden drop in the relative error at the outlet for Run 3.

Analysis of the pressure indicates how well the Navier-Stokes computations represent the irrotational flow outside the boundary layer. Recall that for Blasius flow over a flat plate, $\partial p / \partial x = 0$. Figure 2.6 shows plots of $p(x, y \approx 0.5)$ for the four simulations. Although the pressure varies over the computational domain, it can be seen that the horizontal gradient in the pressure is much less than 1 for all four cases. It is interesting to note that for the cases in which both the horizontal and vertical velocity are specified at the inlet, the pressure at $x-x_o = 0$ has a value of order 10^{-3}. On the other hand, for the case in which only the horizontal velocity is specified at the inlet, the pressure is approximately 10^{-6} at $x-x_o = 0$.
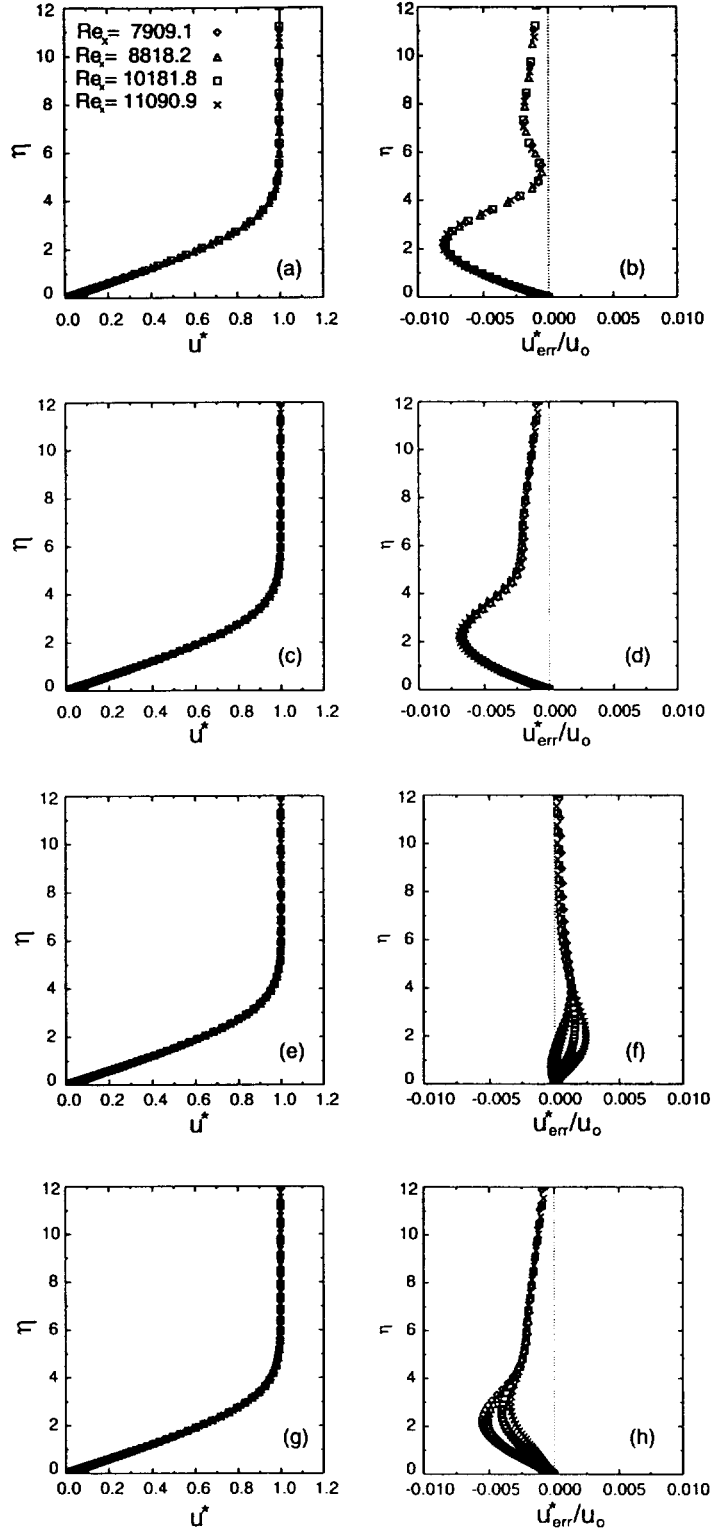
Figure 2.3. Horizontal velocity profiles at various Re_x for (a) Run 1, (c) Run 2, (e) Run 3, and (g) Run 4. Relative difference, $u^*_{err}/u_o = (u^*_{ALE3D}-u^*)/u_o$, between the computed horizontal velocity and the Blasius profile for (b) Run 1, (d) Run 2, (f) Run 3, and (h) Run 4, where $u_o = 1$. The solid line in (a,c,e,g) is u^*.
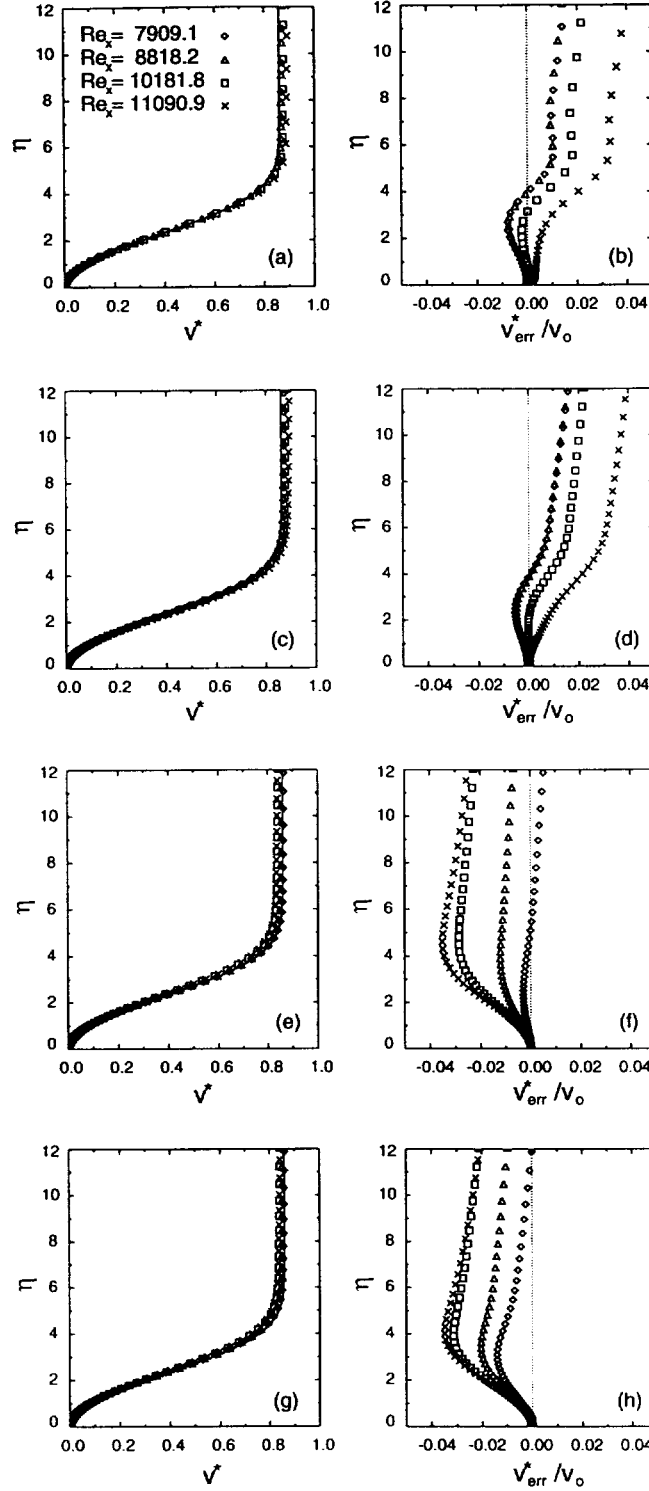
8

Figure 2.4. Vertical velocity profiles at various Re_x for (a) Run 1, (c) Run 2, (e) Run 3, and (g) Run 4. Relative difference, $v^*_{err}/v_o = (v^*_{ALE3D}-v^*)/v_o$, between the computed horizontal velocity and the Blasius profile for (b) Run 1, (d) Run 2, (f) Run 3, and (h) Run 4, where the variable $v_o = 0.860853$ is the value of the vertical velocity outside the boundary layer. The solid line in (a,c,e,g) is v^*.
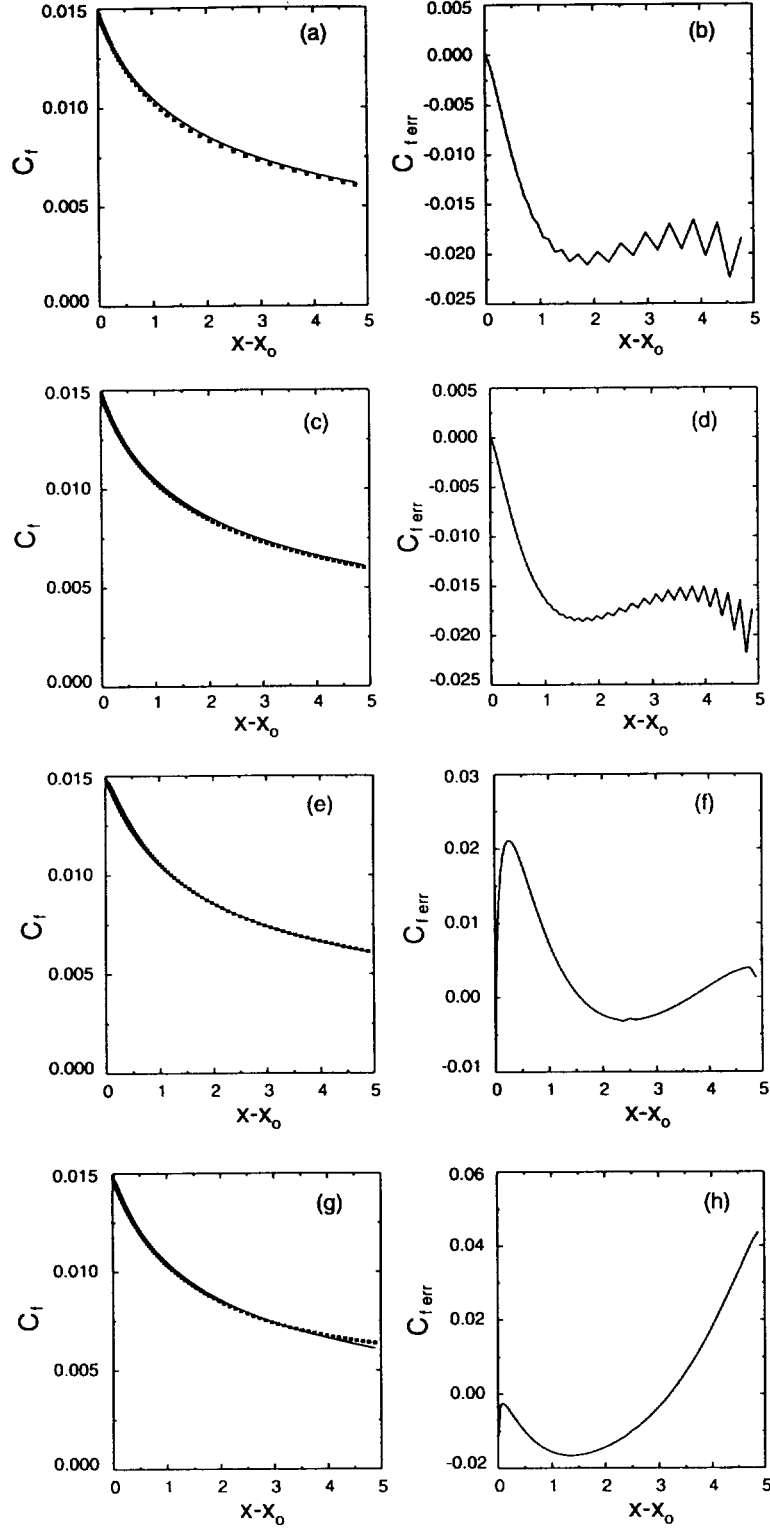
9

Figure 2.5. Shear stress coefficient for (a) Run 1, (c) Run 2, (e) Run 3, and (g) Run 4. Relative difference, $C_{ferr}/C_f = (C_{fALE3D}-C_f)/C_f$, between the computed shear stress coefficient and that of the Blasius solution for (b) Run 1, (d) Run 2, (f) Run 3, and (h) Run 4, The solid line in (a,c,e,g) is C_f.
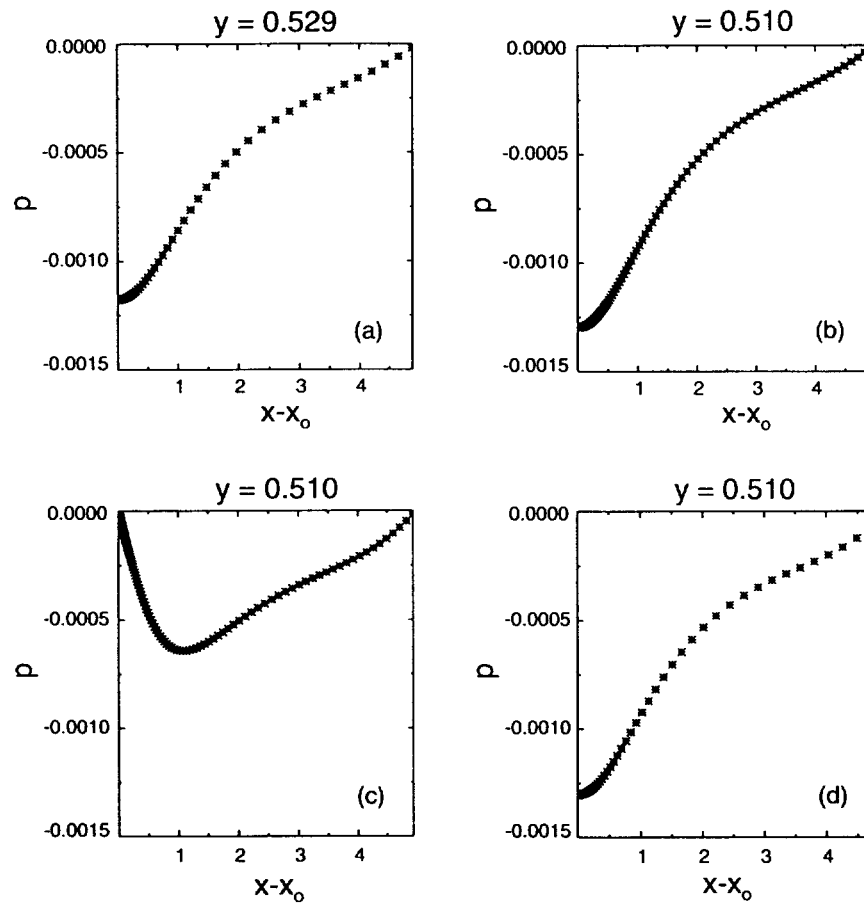
10

Figure 2.6. Pressure vs. x at $y \approx 0.5$ for the (a) Run 1, (b) Run 2, (c) Run 3, and (d) Run 4.

3.0 Flow Over a 2-D Circular Cylinder

The problem of two-dimensional flow about a circular cylinder has been studied quite extensively with experimental, computational, and theoretical techniques. This simple geometry produces a rather complex wake, which makes it a good test case for code benchmarking. For a Reynolds number, Re_d, greater than 4 ($Re_d = Ud/v$, where U is the freestream velocity, d the cylinder diameter, and v the kinematic viscosity of the fluid), the flow about the cylinder separates off of the cylinder's aft face, resulting in two counter-rotating vortices in the immediate wake. When Re_d is increased beyond 60-100, these vortices alternately shed from the cylinder, giving rise to a wake consisting of counter-rotating vortices.

3.1 Computational Setup

The simulations of two-dimensional flow about a circular cylinder are conducted with the incompressible flow model in ALE3D.[1] Two cylindrical grids (Figure 3.1) are employed for these simulations to determine the sensitivity of the results to the grid resolution. The chosen diameter, d, of the cylinder is 1 and the maximum radial dimension of both grids is 32d. To resolve the steep velocity gradients near the cylinder surface and in the cylinder wake, the computational grids are graded in both the radial and azimuthal directions. Table 3.1 lists the details of both grids.

The inlet boundary conditions are such that $(u,v) = (1,0)$ for $r = 32d$ and $90^0 \le \theta \le 270^0$, where u and v are the horizontal and vertical velocity components, respectively. A zero natural boundary condition[1] is imposed at the outlet ($r = 32d$, $-90^\circ \le \theta \le -90^\circ$). Earlier simulations demonstrated that significant flow reversal can occur at the outlet when the flow is well resolved there. Changing either the integration to full Gaussian quadrature or turning hourglass correction on had no effect in eliminating the flow reversal at the outlet. Only coarsening of the grid at the outlet appears to reduce this phenomena from occurring. The mechanisms for this unusual and erroneous flow reversal have not been investigated at the present time. In the subsequent simulations which have a relatively coarse grid at the outlet, this phenomenon is not observed in the flow field. However, this phenomenon may still have some small influence on the calculated results. The out-of-plane velocity component, w, is set to 0 for all nodes and the surface of the cylinder has a no-slip/no-penetration boundary condition ($u = v = 0$). At $t = 0$, the entire flow is initialized with a velocity of $(u,v) = (1,0)$. The code then projects this initial condition to a divergence-free field.[4] To reduce the computational time required for the flow to behave in a quasi-periodic manner, a random velocity perturbation is added to the flow about the cylinder at $t = 0$. Both the CFL number and the diffusion stability number are set to 0.3 for both grids. In the subsequent simulations, the time steps for both coarse and medium grids are diffusion limited. The kinematic viscosity of the fluid is taken to be $v = 0.001$, yielding a $Re_d = 1,000$. The ALE3D input file for these simulations is shown in Appendix 2. The governing equations are solved with a conjugate gradient solver with a tolerance set to 10^{-8}. The explicit time integration scheme is used for both grids. The simulations are run to a point at which the measured

quantities, such as the lift and drag on the cylinder, are behaving in a repeatable manner as the vortices are shed from the cylinder. For the coarse grid, this means running the simulation up to $t \approx 900$ s and, for the medium grid, until $t \approx 275$ s. Post-processing of these simulations is done with Interactive Data Language (IDL) of Research Systems, Inc.
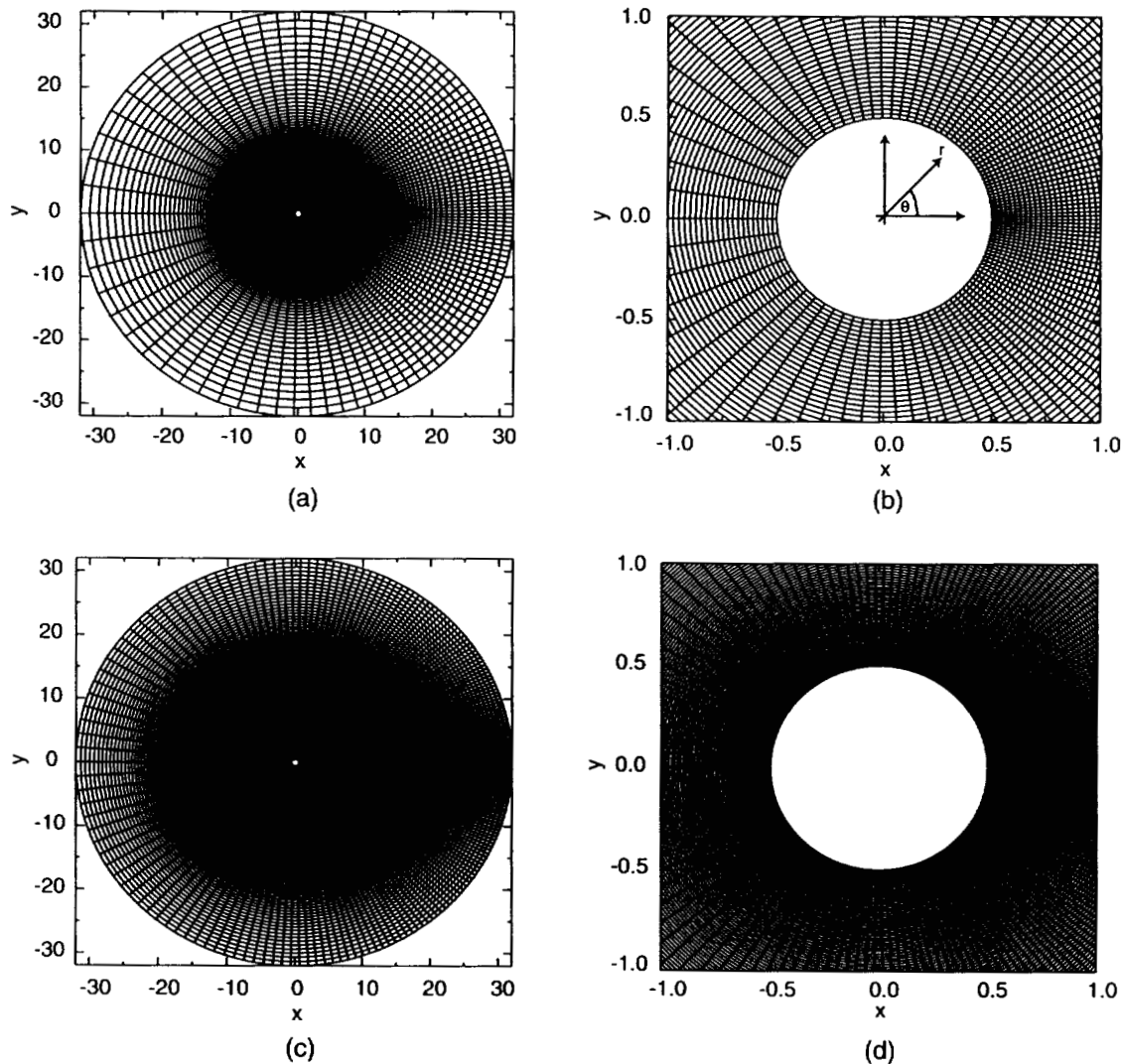

Figure 3.1. Coarse (a) and medium (c) grids used to simulate the flow about a circular cylinder. Close-up views of the (b) coarse and (d) medium grids.

Grid	Total Number of Elements	Number of Elements in r	Number of Elements in θ	Δr_{min}	$\Delta \theta_{min}$ (°)
Coarse	20,000	200	100	0.02169838	1.1638158
Medium	80,000	400	200	0.01082214	0.5764392

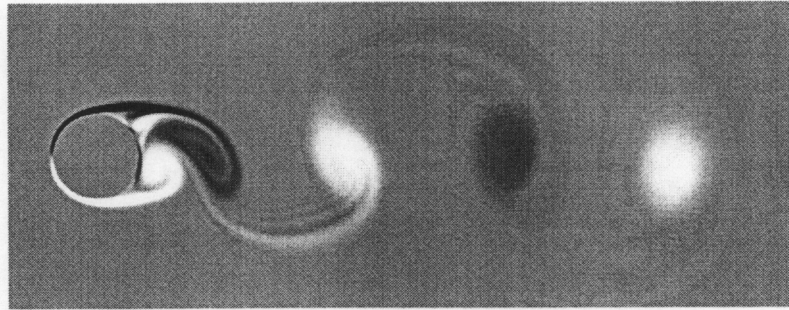Table 3.1. Details of the coarse and medium grids

Figure 3.2. Instantaneous vorticity field about the cylinder for the medium grid. The white color levels indicate positive vorticity and the black color levels negative vorticity.

3.2 Results and Discussion

Figure 3.2 shows an instantaneous vorticity field about the cylinder. The pattern of vortices with alternating senses of rotation in the wake is clearly visible in this figure. This periodic shedding of vorticity results in a periodic variation in both the lift and drag on the cylinder, with the drag varying twice as quickly as the lift. Figure 3.3 shows the drag coefficients ($C_d = D/\left(\frac{1}{2}\rho U^2 d\right)$, where D is the drag force on the cylinder) due to pressure and shear forces throughout both simulations. Note that the total drag, which is the sum of the pressure and shear forces, is due primarily to the pressure forces. The vertical dashed lines in Figure 3.3 indicate the sampling period over which average quantities are calculated. For both grids, this period corresponds to approximately 40 shedding cycles. Figure 3.4 shows the variation of the drag versus time over a small portion of the simulation.

Two important quantities are the average values of the drag coefficient, C_d, and the lift coefficient, $C_l = L/\left(\frac{1}{2}\rho U^2 d\right)$, where L is the lift force on the cylinder. The average values of C_d and C_l are plotted in Figure 3.5 as functions of the number of samples, N, made over the sampling period. It can be seen that for both grids, the amplitude of variation in C_d and C_l decreases with increasing N. Theoretically, C_d and C_l should become independent of N as $N \to \infty$. However, it can be seen that small

amplitude oscillations exist in the average values of C_d and C_l near the end of the sampling period. For the coarse grid, the final amplitude of oscillation in C_d is approximately 0.0005 and that of C_l approximately 0.006. For the fine grid, the final amplitude of oscillation in C_d is approximately 0.0005 and that of C_l approximately 0.007. These oscillations are likely due to the fact that the sampling period is not an integer multiple of the shedding period of vortices in the wake of the cylinder. Further reduction in the amplitude of the oscillation in the average values of C_d and C_l may be achieved by making the sampling period an integer multiple of the shedding period or by increasing the time of the sampling period.

The average values of C_d and C_l are listed in Table 3.2. Table 3.3 shows drag coefficients and Strouhal numbers found in the literature for two-dimensional flow about a circular cylinder at $Re_d = 1,000$. Comparing C_d in Tables 3.2 and 3.3 demonstrates that the average value of C_d from the medium grid is in fair agreement with the values of C_d from the other more recent works on this topic. The average value of C_l should equal zero since, on average, the cylinder generates no net circulation. Although $C_l \neq 0$ in these simulations, the magnitude of C_l is much less than 1. As discussed in the previous paragraph, running these simulations for a longer period of time or making the sampling period an integer multiple of the shedding period would further reduce the magnitude of C_l. Taking the FFT of C_l over the sampling period allows for the calculation of the shedding frequency, f, from which the Strouhal number, $St = fd/U$, can be obtained. Table 3.2 lists the St for both the coarse and medium grids. There is a 4.6% change in St in going from the coarse to the medium grid. The value of St from the medium grid compares favorably with those from other works (Table 3.3).
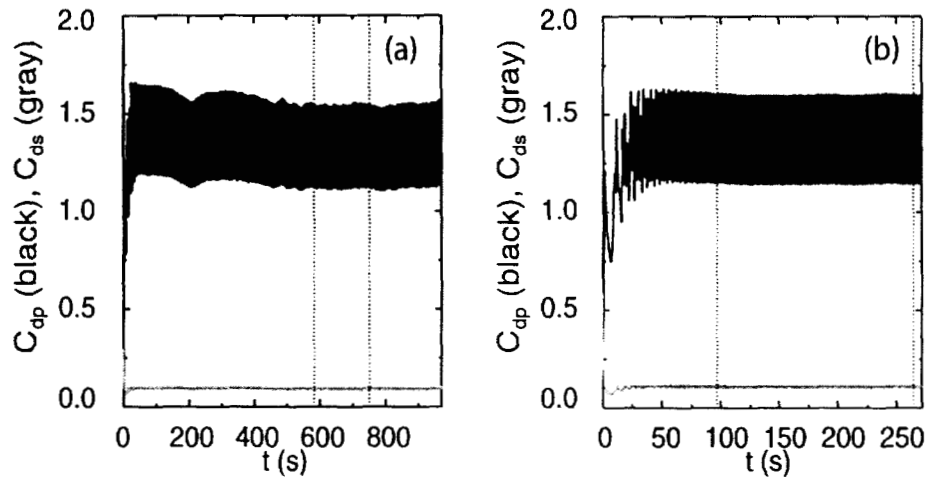

Figure 3.3. Drag coefficients for the (a) coarse and (b) medium grids. C_{dp} (upper black line) is the drag coefficient due to pressure forces and C_{ds} (lower gray line) is that due to shear forces.
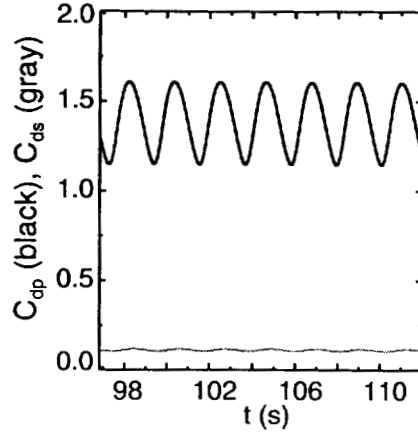
15

Figure 3.4. Drag coefficients for the medium grid over a small portion of the simulation. C_{dp} (upper black line) is the drag coefficient due to pressure forces and C_{ds} (lower gray line) is that due to shear forces.
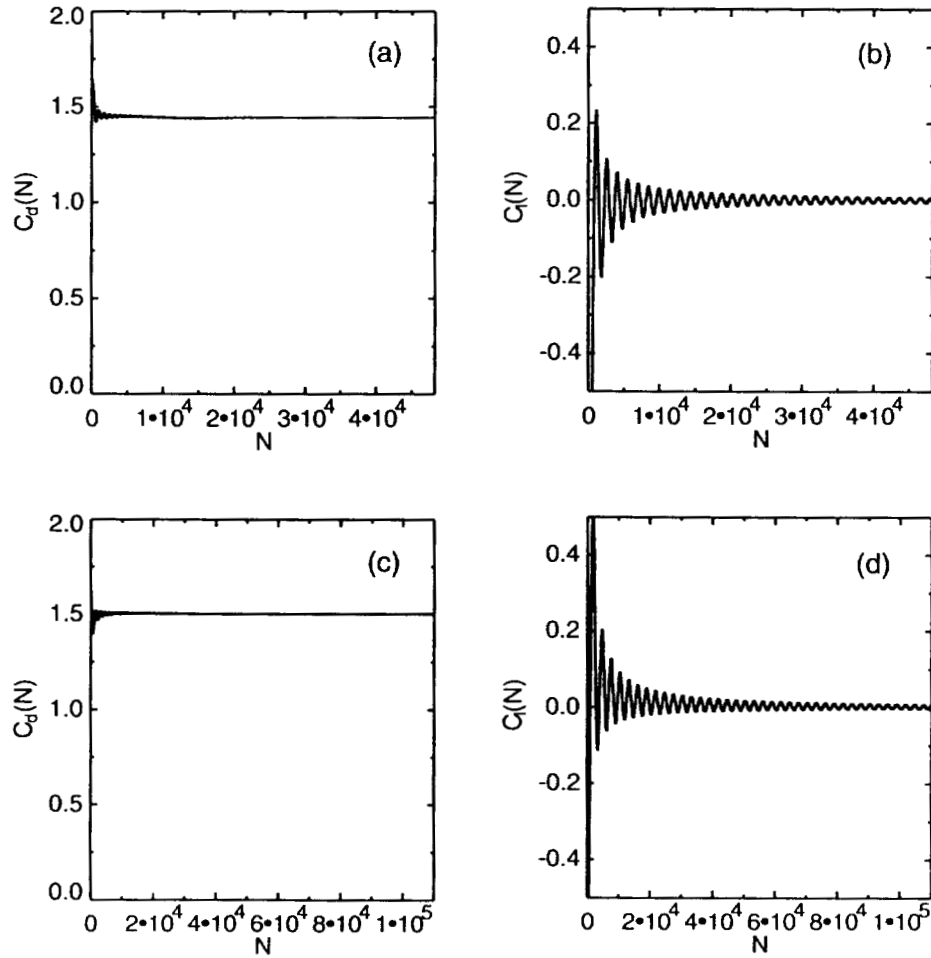

Figure 3.5. Variation of C_d and C_l with the number of samples, N, made during the sampling period for the (a-b) coarse grid and (c-d) medium grid.

An examination of the average flow field in the wake of the cylinder reveals the streamline patterns shown in Figures 3.6-3.7 for the coarse and medium grids. Qualitatively, the average streamlines for both grids appear very similar: the flow forms two separation points, one reattachment point, and three recirculation zones on the upper and lower halves of the cylinder. To provide a more quantitative comparison between the average wake structures for the coarse and medium grids, the separation angle, θ_{sep}, and recirculation length, l_{circ}, are measured. The separation angle is defined to be the angle at which the oncoming flow first detaches from the cylinder, causing the wall shear stress to vanish. The recirculation length is defined to be the distance between the surface of the cylinder and the maximum x value at which the horizontal velocity, $u(x,y=0)$, is identically 0. Figure 3.8 shows a pictorial representation of θ_{sep} and l_{circ}. Table 3.4 shows the θ_{sep} and l_{circ} for the coarse and medium grids. For the coarse grid, there is a distinct asymmetry in the separation angle off of the top and bottom of the cylinder. This may be due to an asymmetric average pressure gradient along the surface of the cylinder or to the possibility that the sampling period is not an integer multiple of the shedding period. This asymmetry in the separation angle is reduced for the medium grid. There is a substantial change in the separation angles (~7.6% for the top separation angle and ~10.3% for the bottom separation angle) and the recirculation lengths (~9.3%) when comparing the results from the coarse and medium grids. These differences may be an indicator that these simulations are not yet grid converged.

4.0 Conclusions

These benchmarking cases demonstrate the performance of the ALE3D incompressible flow model for flow over a flat plate and a two-dimensional circular cylinder. For the flat plate simulation, it is estimated that the implicit time integration scheme results in a twenty-four-fold reduction of the simulation time over that of the explicit time integration scheme. The smallest error in the horizontal velocity occurs for the case in which the implicit time integration scheme is used and the vertical velocity is not specified at the inlet. The errors in the vertical velocity are comparable for all four test cases. For the two explicit time integration cases with the flat plate, a problematic trend is observed. Since the errors in the velocity and shear stress are not significantly reduced through grid refinement, it may not be possible to further reduce the errors. Another problematic trend with the flat plate problem is the sensitivity of the velocity and shear stress to the outlet zero natural boundary condition. For the benchmarking case of a circular cylinder in which an explicit time integration scheme is employed, the drag coefficient and Strouhal number demonstrate convergence to a solution that compares favorably with results from other studies in the literature. Lastly, as these results are only for two specific flow problems, care must be taken when trying to draw conclusions for how well the incompressible flow model in ALE3D simulates other types of flows geometries at different Re.

Acknowledgements

Grid	C_d	C_l	St
Coarse	1.4422	0.0021	0.2279
Medium	1.5022	0.0067	0.2394

Table 3.2. Measurements of the average drag coefficient, C_d, average lift coefficient, C_l, and Strouhal number, St, from the ALE3D simulations.

C_d	St	Reference
1.52	0.24	Qian & Vezza[6]
1.5191	--	He et al.[7]
1.51	--	Blackburn et al.[8]
1.23	0.206	Cheng et al.[9]
1.5091	--	Henderson[10]
1.53	0.241	Behr et al.[11]
1.198	--	Braza et al[12].
1.43	--	Phuoc Loc[13]
1.2	0.21	Roshko[14]

Table 3.3. Drag coefficient, C_d, and Strouhal number, St, measurements for $Re_d = 1,000$ from other studies of flow about a circular cylinder.

18
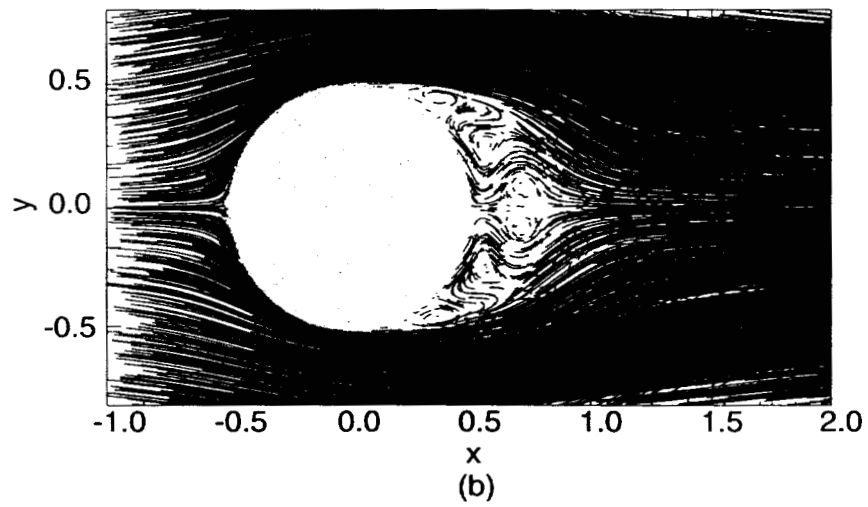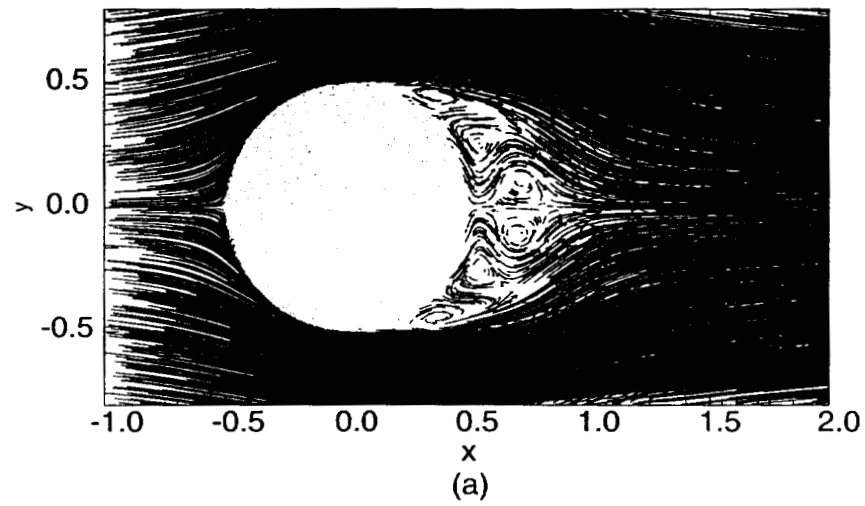
Figure 3.6. Streamlines of the average velocity field about the circular cylinder for the (a) coarse and (b) medium grids.

19
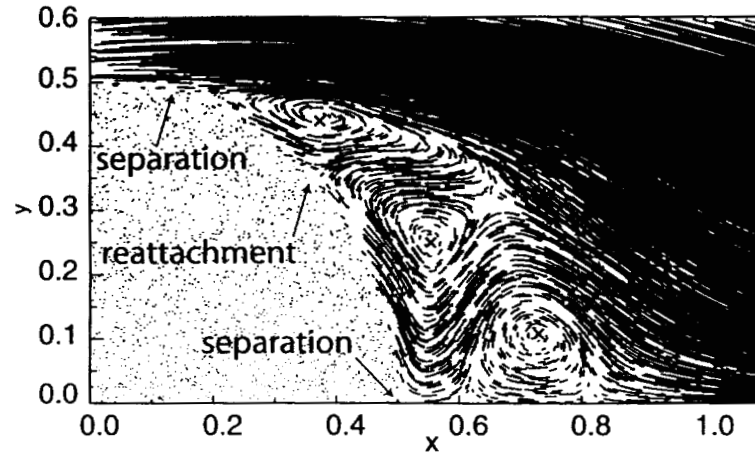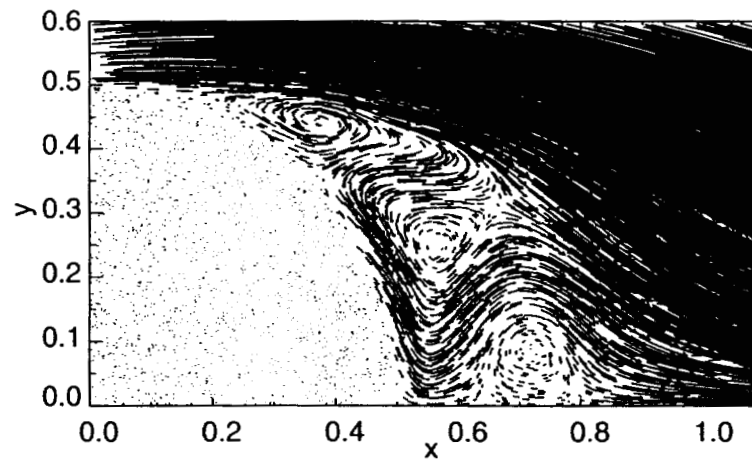
Figure 3.7. Close-up view of the streamlines for the (a) coarse and (b) medium grids. The ×'s in (a) indicate the approximate centers of the recirculation zones.

Grid	$\theta_{sep\ top}$ (°)	$\theta_{sep\ bot}$ (°)	l_{circ}
Coarse	66.084	-64.728	0.290
Medium	71.108	-71.374	0.317

Table 3.4. Separation angles and recirculation length measurements for the coarse and medium grids.
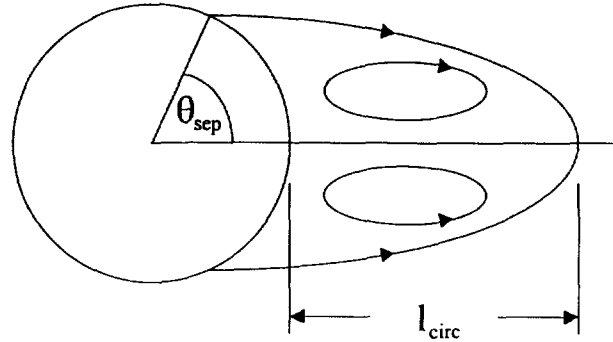
Figure 3.8. Separation angle and recirculation length definitions.

References

1. Dube, E., *et al*. 2001 User's Manual for ALE3D, Version 3.0.0, Lawrence Livermore National Laboratory.
2. Prandtl, L. 1904 *Verhandlunger IIIrd. International Mathematiker Kongresser, Heidelberg*, p. 484. Translation as NASA Memo 452.
3. Blasius, H. 1908 *Z. Angew. Math. Phys.*, **56**, p. 1 (Translation in NACA TM 1256).
4. Gresho, P.M. & Sani, R.L., *Incompressible Flow and the Finite Element Method*, Wiley, 1998.
5. Dunn, T.A. & McCallen, R.C., Parallel Computations of Natural Convection in a Tall Cavity Using an Explicit Finite Element Method, *Int. J. Numer. Meth. Fluids*, 2002, **3**, 1-2.
6. Qian, L. & Vezza, M. 2001 A Vorticity-Based Method for Incompressible Unsteady Viscous Flows, *J. Comp. Phys* **172**, 515-542.
7. He, J.-W., Glowinski, R., Metcalfe, R., Norlander, A., & Periaux, J. 2000 Active Control and Drag Optimization for Flow Past a Circular Cylinder, *J. Comp. Phys.* **163**, 83-117.
8. Blackburn, H.M. & Henderson, R.D. 1999 A Study of Two-Dimensional Flow Past an Oscillating Cylinder, *J. Fluid Mech.* **385**, 255.
9. Cheng, M., Chew, T., & Luo, S.C. 1997 A Hybrid Vortex Method for Flows over a Bluff Body, *Int. J. Numer. Meth. Fluids* **24**, 253.
10. Henderson, R.D. 1997 Nonlinear Dynamics and Patterns in Turbulent Wake Transition, *J. Fluid Mech.* **352**, 65.
11. Behr, M., Liou, R., Shih, R., & Tezduyar, T.E. 1991 Vorticity-stream Function Formulation of Unsteady Incompressible Flow around a Cylinder: Sensitivity of the Computed Flow Field to the Location of the Out Flow Boundary, *Int. J. Numer. Meth. Fluid* **323**.

12. Braza, M., Chassaing, P., & Minh, H.H. 1986 Numerical Study and Physical Analysis of the Pressure and Velocity Fields in the Near Wake of a Circular Cylinder, *J. Fluid Mech.* **165**, 79.

13. Loc, T.P. 1980 Numerical Analysis of Unsteady Secondary Vortices Generated by and Impulsively Started Circular Cylinder, *J. Fluid Mech.* **100**, 111-128.

14. Roshko, A. 1954 *On the Development of Turbulent Wakes from Vortex Sheets,* NACA Report 1191.

Appendix 1 ALE3D Input Files for the Flat Plate

Run 1: Coarse Grid, Explicit Time Step, U_{inlet} and V_{inlet} Specified

```
# flat plate
DECOMP
 partitions 1
END

CONTROL
 stopcycle 100000000
 dtmax 1.
 dtinit 1.e-7
 dtmin 1.e-10
END

OUTPUT
 plotac 0
 dumpcycle 5000 1e9
 plotcycle 5000 1e9
 numcycdigits 6
 notify 1

 plotvar deleteall
 plotvar add p u1 u2 u3

 # tracer_fixed u_watch .95 .01 0.
 # tracer_fixed u_watch0 -1. 0.1 0.
 # tracer_fixed u_watch2 3.7 .2 0.

 # timehist u1 tracer u_watch
 # timehist u1 tracer u_watch0
 # timehist u1 tracer u_watch2
 #timehist inc_rke scalar
END


BOUNDARY
 table const_table 0.0 1.0

 table inlet_profile
  include u1in.txt
 spacetable inst_u1 1.0 y 0.0 table inlet_profile

 table inlet_profile_u2
  include u2in.txt
 spacetable inst_u2 1.0 y 0.0 table inlet_profile_u2

 nodeset fluid material 1
```

22

```
incvelocity fluid 1.0 0.0 0.0


incvel_loadcurve inletu1  spacetable inst_u1 1.0  1.0 0.0 0.0  1  table
const_table

incvel_loadcurve inletu2  spacetable inst_u2 1.0 0.0 1.0 0.0 1 table
const_table


incvel_loadcurve z1      0.0  0.0 0.0 1.0  1  table const_table
incvel_loadcurve z2      0.0  0.0 0.0 1.0  1  table const_table
incvel_loadcurve wall       1.0  0.0 0.0 0.0  0  table const_table


END

HYDRO
 nohydro 1
END

INCFLOW
 inclogiterations 1
 incstabflag 0
 incstabcoef 0.01
 inccfl 0.5
 inccflv 0.5
 inclumpmass 1
 incquadrature 1
 ibtd 1
 ihg 1
 increusesle 1

# solverparams string "minResProjection 10"
# solverparams string "AConjugateProjection 10"
 solverparams
  solverlib hypre
  solver cg
  precond parasails
  parasailssymmetric 1
  parasailsfilter 0.05
  parasailsthreshold 1.e-2
  parasailsnlevels 1
  precond_reuse 1000000
  schurreduction 1
  tol 1.e-12
  maxiter 10000
  outputlevel 0
  debugoutput 0
END


MATERIAL a 1
 incinput rho 1. p0 0.0 mu 0.0005 itrb 0
END
```

Run 2: Medium Grid, Explicit Time Step, U_{inlet} and V_{inlet} Specified

```
# flat plate
DECOMP
 partitions 8
END
```

```
CONTROL
  stopcycle 100000000
  dtmax 1.
  dtinit 1.e-7
  dtmin 1.e-10
END

OUTPUT
  plotac 0
  dumpcycle 5000 1e9
  plotcycle 5000 1e9
  numcycdigits 6
  notify 1

  plotvar deleteall
  plotvar add p u1 u2 u3

  # tracer_fixed u_watch .95 .01 0.
  # tracer_fixed u_watch0 -1. 0.1 0.
  # tracer_fixed u_watch2 3.7 .2 0.

  # timehist u1 tracer u_watch
  # timehist u1 tracer u_watch0
  # timehist u1 tracer u_watch2
  #timehist inc_rke scalar
END


BOUNDARY
  table const_table 0.0 1.0

  table inlet_profile
   include u1in.txt
  spacetable inst_u1 1.0 y 0.0 table inlet_profile

  table inlet_profile_u2
   include u2in.txt
  spacetable inst_u2 1.0 y 0.0 table inlet_profile_u2

  nodeset fluid material 1

  incvelocity fluid 1.0 0.0 0.0


  incvel_loadcurve inletu1  spacetable inst_u1 1.0  1.0 0.0 0.0  1  table
const_table

  incvel_loadcurve inletu2  spacetable inst_u2 1.0 0.0 1.0 0.0 1 table
const_table


  incvel_loadcurve z1      0.0  0.0 0.0 1.0  1  table const_table
  incvel_loadcurve z2      0.0  0.0 0.0 1.0  1  table const_table
  incvel_loadcurve wall       1.0  0.0 0.0 0.0  0  table const_table


END

HYDRO
  nohydro 1
END

INCFLOW
  inclogiterations 1
  incstabflag 0
  incstabcoef 0.01
  inccfl 0.5
  inccflv 0.5
  inclumpmass 1
```

```
  incquadrature 1
  ibtd 1
  ihg 1
  increusesle 1

# solverparams string "minResProjection 10"
# solverparams string "AConjugateProjection 10"
  solverparams
    solverlib hypre
    solver cg
    precond parasails
    parasailssymmetric 1
    parasailsfilter 0.05
    parasailsthreshold 1.e-2
    parasailsnlevels 1
    precond_reuse 1000000
    schurreduction 1
    tol 1.e-12
    maxiter 10000
    outputlevel 0
    debugoutput 0
END


MATERIAL a 1
  incinput rho 1. p0 0.0 mu 0.0005 itrb 0
END
```

Run 3: Medium Grid, Implicit Time Step, U_{inlet} Specified, V_{inlet} Unspecified

```
# flat plate
DECOMP
  partitions 8
END

CONTROL
  stopcycle 100000000
  dtmax 1.
  dtinit 1.e-7
  dtmin 1.e-10
END

OUTPUT
  plotac 0 1 10 20 25 50 100
  dumpac 10 20 25 50
  dumpcycle 100 1e9
  plotcycle 100 1e9
  finaldump 1
  finalplot 0
  numcycdigits 10
  notify 1

  plotvar deleteall
  plotvar add p u1 u2 u3

  tracer_fixed u_watch0 0.01 0.01 0.0
  tracer_fixed u_watch1 1.0  0.01 0.0
  tracer_fixed u_watch2 4.0  0.01 0.0

  timehist u1 tracer u_watch0
  timehist u1 tracer u_watch1
  timehist u1 tracer u_watch2
  timehist inc_rke scalar
  timehist inc_divergence scalar
```

END

BOUNDARY
 table const_table 0.0 1.0

 table inlet_profile
  include u1in.txt
 spacetable inst_u1 1.0 y 0.0 table inlet_profile

 nodeset fluid material 1

 incvelocity fluid 1.0 0.0 0.0

 incvel_loadcurve inletu1 spacetable inst_u1 1.0 1.0 0.0 0.0 1 table const_table

 incvel_loadcurve z1   0.0 0.0 0.0 1.0 1 table const_table
 incvel_loadcurve z2   0.0 0.0 0.0 1.0 1 table const_table
 incvel_loadcurve wall   1.0 0.0 0.0 0.0 0 table const_table

END

HYDRO
 nohydro 1
END

INCFLOW
parameters needed for 2D implicit runs
 incmethod implicit
 inctime 1
for 2d problems
 inc2d 1
thetak and thetan (if both 1, then fully implicit)
note: if fully implicit, solve velocity with gmres (nonsym)
if semi implicit, OK to use cg for velocity (sym)
 ifthetak 1.0
 ifthetan 1.0
The diffusion courant limit is set to a big number
 inccfl 3.
 inccflv 1.0e6
 inclumpmass 0
btd is turned off but may be needed for some cases
 ibtd 0
 ebtd 0.375
 incresetppeguess 0
This makes sure you don't use the u-guess for v etc.
but instead use the previous values
 incresetvelguess 1

inclogiterations 1
 incstabflag 0
 incstabcoef 0.01
We want quadrature to be 8 for implicit
 incquadrature 8

 incdivcalc 1
 irke 1
 incdivfree 1

Solver params needed for implicit solve
solverparams ppe string "minResProjection 10"
 solverparams ppe
  solverlib hypre
  schurreduction 1
  solver cg

```
      precond parasails
      parasailssymmetric 1
      parasailsfilter 0.05
      parasailsthreshold 1.e-2
      parasailsnlevels 1
      precond_reuse 1000000
      tol 1.e-12
      maxiter 10000
      outputlevel 0
      debugoutput 0

    solverparams vel
      solverlib hypre
      solver gmres
      precond diag
      gmresdim 1000
      maxiter 5000
      tol 1.e-12
      outputlevel 0

  END


  MATERIAL a 1
    incinput rho 1. p0 0.0 mu 0.0005 itrb 0
  END
```

Run 4: Medium Grid, Implicit Time Step, U_{inlet} and V_{inlet} Specified

```
# flat plate
 DECOMP
# partitions 8
 END

CONTROL
  stopcycle 100000000
  dtmax 1.
  dtinit 1.e-7
  dtmin 1.e-10
END

OUTPUT
  plotac 0 1 2 3 4 5 10 20 25 50 100
  dumpac 10 20 25 50
  dumpcycle 100 1e9
  plotcycle 100 1e9
  finaldump 1
  finalplot 0
  numcycdigits 10
  notify 1

  plotvar deleteall
  plotvar add p u1 u2 u3

  tracer_fixed u_watch0 0.01 0.01 0.0
  tracer_fixed u_watch1 1.0  0.01 0.0
  tracer_fixed u_watch2 4.0  0.01 0.0

  timehist u1 tracer u_watch0
  timehist u1 tracer u_watch1
  timehist u1 tracer u_watch2
  timehist u2 tracer u_watch0
  timehist u2 tracer u_watch1
```

```
        timehist u2 tracer u_watch2
        timehist inc_rke scalar
        timehist inc_divergence scalar
END


BOUNDARY
    table const_table 0.0 1.0

    table inlet_profile
     include u1in.txt
    spacetable inst_u1 1.0 y 0.0 table inlet_profile

    table inlet_profile_u2
     include u2in.txt
    spacetable inst_u2 1.0 y 0.0 table inlet_profile_u2

    nodeset fluid material 1

    incvelocity fluid spacetable inst_u1  1.0 0.0 0.0

    incvel_loadcurve inletu1  spacetable inst_u1 1.0  1.0 0.0 0.0  1 table
const_table

    incvel_loadcurve inletu2  spacetable inst_u2 1.0 0.0 1.0 0.0 1 table
const_table


    incvel_loadcurve z1      0.0  0.0 0.0 1.0  1  table const_table
    incvel_loadcurve z2      0.0  0.0 0.0 1.0  1  table const_table
    incvel_loadcurve wall        1.0  0.0 0.0 0.0  0  table const_table


END

HYDRO
    nohydro 1
END

INCFLOW
# parameters needed for 2D implicit runs
  incmethod implicit
  inctime 1
# for 2d problems
  inc2d 1
# thetak and thetan (if both 1, then fully implicit)
# note: if fully implicit, solve velocity with gmres (nonsym)
#      if semi implicit, OK to use cg for velocity (sym)
  ifthetak 1.0
  ifthetan 1.0
# The diffusion courant limit is set to a big number
  inccfl 3.
  inccflv 1.e6
  inclumpmass 0
# btd is turned off but may be needed for some cases
  ibtd 0
  ebtd 0.375
  incresetppeguess 0
# This makes sure you don't use the u-guess for v etc.
# but instead use the previous values
  incresetvelguess 1

inclogiterations 1
  incstabflag 0
  incstabcoef 0.01
# We want quadrature to be 8 for implicit
  incquadrature 8

  incdivcalc 1
  irke 1
```

```
    incdivfree 1

  # Solver params needed for implicit solve
  solverparams ppe string "minResProjection 10"
   solverparams ppe
     solverlib hypre
     schurreduction 1
     solver cg
     precond parasails
     parasailssymmetric 1
     parasailsfilter 0.05
     parasailsthreshold 1.e-2
     parasailsnlevels 1
     precond_reuse 1000000
     tol 1.e-12
     maxiter 10000
     outputlevel 0
     debugoutput 0

   solverparams vel
     solverlib hypre
     solver gmres
     precond diag
     gmresdim 1000
     maxiter 5000
     tol 1.e-12
     outputlevel 0

  END


  MATERIAL a 1
   incinput rho 1. p0 0.0 mu 0.0005 itrb 0
  END
```

Appendix 2 ALE3D Input File for the Circular Cylinder

Coarse and Medium Grids

```
# circle

DECOMP
 partitions 16
END

CONTROL
 stopcycle 1000000
 #stoptime 10.0
 dtmax 1.
 dtinit 1.e-5
 dtmin 1.e-10
END

OUTPUT
 plotac 0
 #plottime 0.1 1.e9
 #finaldump 1
 #finalplot 0
 dumpcycle 5000 1e9
 plotcycle 2000 1e9

 numcycdigits 6
 notify 10
```

```
derivedvar dragc nodeset pr1 scale 1. inc_fx
derivedvar liftc nodeset pr1 scale 1. inc_fy
derivedvar dragp nodeset pr1 scale 1. inc_fxp
derivedvar liftp nodeset pr1 scale 1. inc_fyp
derivedvar drags nodeset pr1 scale 1. inc_fxs
derivedvar lifts nodeset pr1 scale 1. inc_fys

timehist_truncrestart 0
timehist dragc sum
timehist liftc sum
timehist dragp sum
timehist liftp sum
timehist drags sum
timehist lifts sum
timehist inc_rke scalar
timehist inc_divergence scalar

tracer_fixed v_time0 4.0 0.0 0.0
timehist u2 tracer v_time0

tracer_fixed p_time0 0.5 0.0 0.0
timehist p tracer p_time0


plotvar deleteall
plotvar add p u1 u2 u3
plotvar add incta_u incta_v incta_p
plotvar add uvortz
END

BOUNDARY
table const_table 0.0 1.0
nodeset lefthalf boundingbox -100. -100. -100. 0. 100. 100. 1.e-2
nodeset inlet intersection pr2 lefthalf
nodeset blob filledcyl 0. 0. -100. 0. 0. 100. 1. 1.e-1
incvel_loadcurve inlet   1.0   1.0 0.0 0.0   0   table const_table
incvel_loadcurve pr1     0.0   1.0 1.0 1.0   1   table const_table
incvel_loadcurve pz1     0.0   0.0 0.0 1.0   1   table const_table
incvel_loadcurve pz2     0.0   0.0 0.0 1.0   1   table const_table
incvelocity nall 1.0 0.0 0.0
incperturb blob 0 0.3 0.3 0.0
END

INCFLOW
incnodalforce 1
irke 1
ivort 1
itavg u v
incdivcalc 1
inclogiterations 1
incstabflag 1
incstabcoef 0.01
inccfl 0.3
inccflv 0.3
increusesle 1

solverparams string "minResProjection 10"
solverparams
 solverlib hypre
 solver cg
 precond parasails
 parasailssymmetric 1
 parasailsfilter 0.05
 parasailsthreshold 1.e-2
 parasailsnlevels 1
 precond_reuse 1000000
 schurreduction 1
 tol 1.e-8
 maxiter 10000
```

```
    outputlevel 0
    debugoutput 0
END

MATERIAL fluid 1
  incinput rho 1.0 p0 0.0 rnu 0.001
END
```